Disponible en ligne sur
ScienceDirect
www.sciencedirect.com
Elsevier Masson France
EM|consulte
www.em-consulte.com
IRBM
IRBM 39 (2018) 43–53

Original Article

Neutrosophic Based Nakagami Total Variation Method for Speckle Suppression in Thyroid Ultrasound Images

D. Koundal [a,b,*], S. Gupta [b], S. Singh [b]

[a] *Department of Computer Science & Engineering, Chitkara University Institute of Engineering & Technology, Chitkara University, Baddi, Himachal Pradesh, India*

[b] *Department of Computer Science & Engineering, University Institute of Engineering & Technology, Panjab University, Chandigarh, Punjab, India*

Received 29 July 2017; received in revised form 8 November 2017; accepted 8 November 2017
Available online 27 November 2017

Highlights

- The Neutrosophic based Nakagami based Total Variation (NTV) method has been proposed.
- It can make balance between speckle reduction and edge preservation.
- It is able to handle the indeterminate pixels and preserve the valuable information such as texture and edges.
- It can assist endocrinologists in improving the quality of ultrasound images for accurate segmentation of thyroid nodules.

Graphical abstract

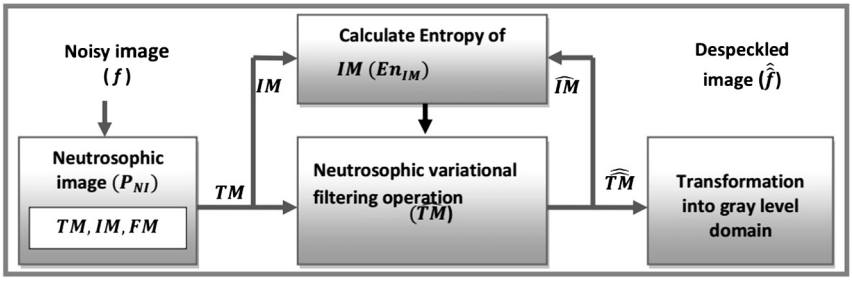

Abstract

Background: Neutrosophic based methods are becoming very popular in denoising of images due to the capability of handling indeterminacy. The main goal of denoising is to maintain balance between edge preservation and speckle reduction.
Methods: To achieve this, neutrosophic based total variation method using Nakagami statistics have been explored to develop an efficient speckle reduction method. The proposed Neutrosophic based Nakagami Total Variation (NNTV) method initially transforms the image into the neutrosophic domain and then employs the neutrosophic filtering process for speckle reduction. The NNTV quantifies the indeterminacy of image by determining the entropy of indeterminate set.
Results: The performance of the proposed method has been evaluated quantitatively by quality metrics on synthetic images, qualitatively using real thyroid ultrasound images through visual examination by medical experts and by Mean Opinion Score.
Conclusion: From results, it has been observed that NNTV method performed better than other speckle reduction methods in terms of both speckle suppression and edge preservation.

* Corresponding author.
E-mail addresses: deepika.koundal@chitkara.edu.in (D. Koundal), savita2k8@pu.ac.in (S. Gupta), sukhdalip@pu.ac.in (S. Singh).

https://doi.org/10.1016/j.irbm.2017.11.003
1959-0318/

Keywords: Nakagami distribution; Ultrasound images; Speckle reduction; Edge preservation; Neutrosophy; Total variation

1. Introduction

Ultrasound image is commonly used for earlier detection of thyroid nodules. It is generally preferred due to its non-ionising radiation effects, inexpensive and painless scanning operations which provide diagnostically important information needed for medical diagnosis [1]. However, the key challenge in automated analysis using ultrasound images is to delineate accurate nodules within the thyroid gland due to the existence of speckle noise and intensity in-homogeneity. Speckle noise considerably reduces the image quality and thus makes the differentiation of fine details difficult. The aim of speckle removal method is to enhance the quality of ultrasound images for the accurate segmentation of thyroid nodules [2,31]. However, the speckle removal is always a trade-off between noise suppression and edge preservation.

Number of efforts have been attempted for the removal of speckle noise using variational methods [3–7]. Total variation based methods consist of data term that is estimated from noise distribution and regularization term that is utilized for edge preservation. Rudin et al. introduced a first variational based speckle reduction method which consisted of non-convex fidelity term with Gaussian noise distribution [3]. Another non-convex model known as Aubert–Aujol (AA) model which is used for speckle reduction is introduced by Aubert et al. followed the gamma statistics in Maximum a Posteriori (MAP) probability framework [4]. Further, Shi et al. used the fidelity term of AA model that is transformed from multiplicative problem into the additive one [5]. This model is known as Shi–Osher (SO) model that is strictly convex. In [6], another non-convex model is introduced for speckle reduction using gamma statistics by the MAP estimation in log domain. One of the variational methods based on Nakagami distribution has been presented by Koundal et al. for the reduction of speckle noise in ultrasound images [7]. From preliminary results of [7], it has been observed that the Nakagami Total Variation (NTV) method is able to preserve edges well but not the texture information.

Moreover, variational methods often suffer from staircase effects due to the loss of local features like texture and small details in form of residue. Total variation (TV) is an effective method but often fails to preserve very fine texture details, which may resemble the granular pattern of speckle due to the presence of fuzziness caused by texture patterns in ultrasound images. Therefore, texture information is often misinterpreted as speckle and suppressed along with speckle noise. The TV methods often suppress indeterminate pixels mistakenly along with other significant diagnostic information instead of their preservation. Moreover, indeterminacy of image has been ignored in most of the traditional speckle reduction methods.

To address this issue, fuzzy domain is most widely used by the researchers to handle the fuzziness of images [8]. However, fuzzy set can handle only the membership degree but fails to deal with non-membership and indeterminacy degree of pixels. Recently, the Neutrosophic Set (NS), which is the generalization of fuzzy set is becoming popular in image processing applications [9]. Many researchers have used NS in image denoising applications which have shown that neutrosophic based methods yield good performance due to their indeterminacy handling capability [10–21].

The goal is to preserve texture details which have high indeterminacy degree due to resemblance to the speckle noise. To achieve balance between speckle suppression and texture preservation, the Nakagami based Total Variation (NTV) method presented in [7] has been further explored in Neutrosophic domain. No work has been published on speckle removal of ultrasound images using Nakagami statistics in neutrosophic domain. Thus, an effort has been made to develop a Neutrosophic based Nakagami Total Variation (NNTV) method using Nakagami statistics in neutrosophic domain for removing speckle noise in thyroid ultrasound images. It initially transforms the image into the neutrosophic domain and then employs the Nakagami based neutrosophic filtering process for speckle removal and edge preservation. The NNTV quantifies the indeterminacy of image by determining the entropy of indeterminate set.

2. Related work on neutrosophic domain speckle reduction methods

Several denoising methods based on neutrosophic set have been presented in the literature to remove Salt & Pepper, Gaussian, speckle and Rician noise [10,12,20]. Various notions and theories based on NS filter are defined and applied for image denoising.

Guo et al. introduced the neutrosophic based method to remove Salt & Pepper noise and Gaussian noise with different variances [10,11]. Mohan et al. has presented various methods for the removal of Rician noise using Magnetic Resonance (MR) image in literature [12,13]. One of the methods is based on Neutrosophic set (NS) using median filtering [12]. The γ-median filtering operation is employed on True subset and False subset for the reduction of indeterminacy for the removal of noise [13]. The filter outperformed the median and the classical Non Local Mean method for different noise levels. Further, Mohan et al. introduced a wiener filter in neutrosophic domain for the removal of Rician noise [14,15]. The wiener filtering operation is employed on true and false subsets for the reduction of noise and indeterminacy. The experiments have been performed on simulated MRI from Brainweb database and clinical MR images [16]. In [17], the Wiener method based on Non Local Neutrosophic Set (NLNS) is introduced for the removal of Rician noise from MRI. First, the nonlocal mean is applied to the noisy MRI. Then, the resultant image is transformed into NS domain and entropy of the neutrosophic set is quantified to estimate the indeterminacy. The experimental results have shown

that the NLNS wiener filter in neutrosophic domain produced better denoising results in terms of both quantitative and qualitative measures in comparison to the anisotropic diffusion filter, Wiener filter, the nonlocal means filter and the total variation minimization.

In [18], an approach is introduced on the basis of neutrosophic filtering with the integration of level set. The image is mapped into NS domain and described using three membership sets. The Directional Alpha-Mean Filter (DAMF) is employed for the reduction of image indeterminacy which is then segmented by level set algorithm. The experimental results had revealed that the method performed better due to indeterminacy handling capability. Xianying et al. introduced a pixel-wise adaptive neutrosophic filter for the reduction of high-level Salt-and-Pepper noise. The method is based on neutrosophic indeterminacy feature. In this, the pixel indeterminacy is measured by a Neutrosophic Set and exploited to determine the similarity of pixels. The extensive experiments on several images demonstrated that with a 3 × 3 window, the method outperformed many other denoising methods in terms of preserving details and suppressing noise [18].

Very few neutrosophic domain denoising methods are reported for the removal of Salt & pepper noise, Gamma noise, Gaussian noise and Rician noise in the literature so far. However, a very little work has been published for the speckle removal based on noise statistics in ultrasound images using neutrosophic domain. In [20], another neutrosophic domain based speckle noise reduction method is presented which is based on Gamma noise distribution. In [21], LEE filter [22] and KUAN filter [23] were implemented in neutrosophic domain for the reduction of speckle noise. The experiments have shown that NLEE filter and NKUAN filter outperformed the LEE and KUAN filter on artificial image simulated by speckle noise with different levels of noise. The visual comparison of images indicated that the NLEE and NKUAN suppressed the speckle noise well while preserving the edges. The results using the speckle reduction filters in neutrosophic domain are found better with respect to the previous approaches in the literature.

Therefore, a new Neutrosophic domain Nakagami Total Variation (NNTV) has been proposed for speckle reduction in thyroid ultrasound images by getting motivated from the preliminary results of NTV method so that a good balance can be made between speckle suppression and texture preservation [7].

3. Material and methods

3.1. Material

3.1.1. Dataset

In this research work, synthetic and real ultrasound images have been used for the validation of NNTV method. For the analysis of speckle suppression method, three "noise free" test images are obtained from the home page of Aleksandra Pizurica [24]. These test images include synthetic image, phantom image and realistic ultrasound image (in which speckle was suppressed). More test images are generated by simulating the test images with speckle noise using speckle simulation procedure [20]. In this process, 21 images are generated by adding speckle noise with different values of standard deviation ($\sigma = 0.3$, 0.4, 0.5, 0.6, 0.7, 0.8 and 0.9). These images have been used only for evaluating the speckle suppression methods. The real thyroid ultrasound images are acquired from the Department of Radiology, Post Graduate Institute of Medical Education & Research (PGIMER), Chandigarh, India, for retrospective study. It consists of 50 subjects, out of which, 20 were males and 30 were females, age ranging from 15–70 years. The images are of size 628 × 656 pixels, which were acquired with a 256 grey-level depth using IU22 Philips X Matrix with linear probe at a frequency of 17.5 MHz.

3.1.2. Performance measures

For the performance evaluation of speckle reduction methods, some aspects such as edge preservation and speckle suppression are taken into account. The calculation of image quality measures requires ground truth image, noisy image and a despeckled image. The evaluation metrics for the evaluation purpose are described as follows:

i. Signal-to-noise ratio (SNR)

The signal-to-noise ratio is the ratio of noise free image variance to the error variance between noise free image and processed image. It is computed as

$$\mathrm{SNR} = 10\log_{10}\left(\frac{\sigma_z^2}{\sigma_e^2}\right) \tag{1}$$

where σ_z^2 is the noise-free reference image variance and σ_e^2 is the error variance (between the original and denoised image) [24].

ii. Visual information fidelity (VIF)

Visual information fidelity correlates fidelity of image to the amount of information that is mutual between two images. VIF partitioned the image into several blocks at every sub-band. VIF is represented as

$$VIF = \frac{\sum j \in subbands\ I(C^{N,J}; F^{N,J}S^{N,J})}{\sum j \in subbands\ I(C^{N,J}; E^{N,J}S^{N,J})} \tag{2}$$

where, numerator signifies the information presented in all sub bands of the estimated image and denominator term denotes the information in the reference image [25].

iii. Universal quality index (UQI)

UQI is used to measure the image distortion as a combination of correlation loss, luminance distortion and contrast distortion instead of traditional error summation methods.

$$UQI = \frac{\sigma_{zf}}{\sigma_z\sigma_f}\frac{2\bar{z}\bar{f}}{(\bar{z})+(\bar{f})}\frac{2\sigma_z\sigma_f}{\sigma_z^2+\sigma_f^2}, \quad -1 < UQI < 1 \tag{3}$$

The first part of equation is correlation loss which represents the correlation coefficient to determine the relationship between

original and filtered image. The second part is luminance distortion which measures the similarity in the luminance between two images [26]. The last part is contrast distortion which computes the similarity in the contrasts of original and denoised images, respectively.

iv. Edge preservation index (EPI)

The EPI can be represented as

$$EPI = \frac{\sum(\Delta z - \overline{\Delta z})(\Delta f - \overline{\Delta f})}{\sum(\Delta z - \overline{\Delta z})^2(\Delta f - \overline{\Delta f})^2} \quad (4)$$

where Δz and Δf are the filtered versions of z and f achieved with a 3×3 pixel standard approximation of the Laplacian operator [27]. The $\overline{\Delta z}$ and $\overline{\Delta f}$ are the mean values of the high pass filtered versions of Δz and Δf respectively.

v. Multiscale-structural similarity index metric (MSSIM)

The Structural Similarity Index metric (SSIM) is a perception-based model that takes into account the image degradation as a perceived variation in structural information with the incorporation of contrast masking and luminance masking terms. Contrast masking is a phenomenon where distortions become less noticeable in textured regions of image. Luminance masking is a phenomena where image degradations tends to less visible in bright regions. The SSIM between two images is represented as:

$$SSIM(z, f) = \frac{(2\mu_z\mu_f + 2.55)(2\sigma_{zf} + 7.65)}{(\mu_z^2 + \mu_f^2 + 2.55)(\sigma_z^2 + \sigma_f^2 + 7.65)},$$
$$-1 < SSIM < 1 \quad (5)$$

The MSSIM is used for the evaluation of the overall image quality.

$$MSSIM(z, f) = \frac{1}{M_w}\sum_{j=1}^{M} SSIM(z_j, f_j) \quad (6)$$

where z and f are the original and denoised images, respectively. z_j and f_j are the image contents at the jth local window and M_w is the number of local windows of the image, μ_z is the average of z, μ_f is the average of f, σ_z^2 is the variance of z, σ_f^2 is the variance of f and σ_{zf} is the covariance of z and f [28].

3.2. Methods

3.2.1. Neutrosophy

Smarandache introduced Neutrosophy as a new way to deal with the scope of neutralities and nature [29]. Neutrosophic theory presents a general framework to deal with indeterminacy. It generalizes the fuzzy logic and handles the contradictions, antinomies, paradoxes and antitheses [29]. It takes into account every proposition, concept, theory, entity, or event $\langle A \rangle$ associate to its converse $\langle Anti\text{-}A \rangle$, the neutralities $\langle Neut\text{-}A \rangle$ and which is not $A\langle Non\text{-}A \rangle$ is neither $\langle A \rangle$ nor $\langle Anti\text{-}A \rangle$. The $\langle Neut\text{-}A \rangle$ and $\langle Anti\text{-}A \rangle$ are denoted as $\langle Non\text{-}A \rangle$ [11].

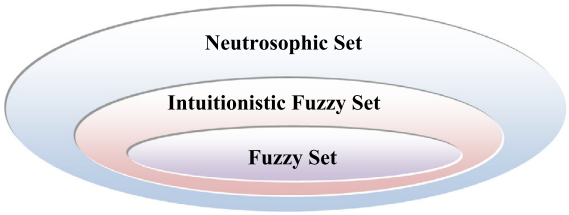

Fig. 1. Relationship among fuzzy set, intuitionistic fuzzy set and neutrosophic set [30].

Neutrosophic Set (NS) is a branch of Neutrosophy theory, which generalizes the concept of the classic set, fuzzy set, paradoxist set, intuitionistic fuzzy set, interval valued fuzzy set and tautological set. Neutrosophic Set is represented as Truth Membership (*TM*), Indeterminacy Membership (*IM*) and Falsity Membership (*FM*) independently. In neutrosophic logic, three neutrosophic components: *TM*, *IM*, *FM* are defined to estimate the degree of truth, the degree of indeterminacy (neither true nor false) and the degree of false [11]. Unlike fuzzy logic, neutrosophic logic introduces the extra domain *IM* that provides a more efficient way to handle higher degrees of indeterminacy that are very difficult to be handled by fuzzy logic. The relationship among fuzzy set, intuitionistic fuzzy set and neutrosophic set is shown in Fig. 1. In case of classical set, *TM* and *FM* have either 0 or 1 values and $IM = \emptyset$. While in fuzzy set, $IM = \emptyset$ but *TM* and *FM* are real numbers $\in [0, 1]$ and sum of *TM* and *FM* must be equal to 1. In neutrosophic set, there is no limit on the sum of *TM*, *IM* and *FM* that is *TM*, *IM*, $FM \in]^-0, 1^+[$.

Neutrosophic image: *A neutrosophic image P_{NI} is composed of bright pixels and characterized by three subsets TM, IM and FM [15]. Pixel in neutrosophic domain can be characterized as P_{NI} $\{t_m, i_m, f_m\}$, representing the pixel as t_m% true (nodule), i_m% indeterminate (nodule boundaries) and f_m% false (background), where $t_m \in TM$, $i_m \in IM$, and $f_m \in FM$ [16].*

3.2.2. Proposed speckle reduction method

Fig. 2 shows the block diagram of neutrosophic domain speckle reduction method. The proposed method first transformed the image into the neutrosophic domain. Second, entropy is determined to deal with the indeterminacy and then the proposed filtering operation is applied. Last, the image is transformed back into spatial domain from neutrosophic domain.

A. Transformation of image in neutrosophic domain

In neutrosophic domain *TM*, *IM* and *FM* are the neutrosophic components used to represent $\langle A \rangle$, $\langle Neut\text{-}A \rangle$ and $\langle Anti\text{-}A \rangle$ respectively. Every neutrosophic pixel can be represented as $P_{NI} = \{TM, IM, FM\}$, where *TM*, *IM* and *FM* are the set of white pixels, indeterminate pixels and non-white pixels respectively [15]. The membership functions *TM*, *IM* and *FM* are computed as given below:

$$TM = \frac{\hat{f}_{ij} - \hat{f}_{\min}}{\hat{f}_{\max}} \quad (7)$$

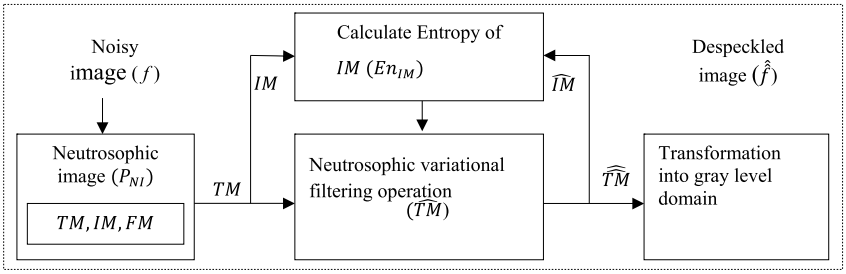

Fig. 2. Block diagram of neutrosophic domain speckle reduction method.

where i differs from 0 to $n-1$, j differs from 0 to $m-1$, $\hat{f}_{ij}$ is local mean obtained using window, $\hat{f}_{\min}$ is minimum intensity value and $\hat{f}_{\max}$ is the maximum intensity value [10].

$$\hat{f}_{ij} = \frac{1}{w \times w} \sum_{m=i-\frac{w}{2}}^{i+\frac{w}{2}} \sum_{n=j-\frac{w}{2}}^{j+\frac{w}{2}} f_{mn} \tag{8}$$

where f_{mn} is the noisy image, $\hat{f}_{ij}$ is pixel's local mean on a window and w is size of window. In experiments, the window size w is selected to be 5 that are found optimum in terms of both feature preservation and speckle suppression through experimental investigations [11].

$$IM = \frac{\delta_{ij} - \delta_{\min}}{\delta_{\max}} \tag{9}$$

$$\delta_{ij} = abs(f_{ij} - \hat{f}_{ij}) \tag{10}$$

where δ_{ij} is absolute difference value between local mean value $\hat{f}_{ij}$ and intensity f_{ij}, $\delta_{\max}$ is the maximum absolute difference value and $\delta_{\min}$ is minimum absolute difference value [12]. The false membership is computed as

$$FM = 1 - TM \tag{11}$$

The true subset, TM, is computed by normalizing the intensity values in [0, 1] as given in Eq. (7). In ultrasound images, pixels belonging to speckle and texture are hard to differentiate, therefore, neighbourhood mean, $\hat{f}_{ij}$, is calculated to ascertain the local mean of pixels in a window [13–17]. The absolute difference is used to determine the indeterminate component. False subset, FM, is computed as the complement of TM [18].

B. Neutrosophic entropy

The neutrosophic entropy is used to quantify degree of indeterminacy in images by considering the way in which uncertainities are captured. The neutrosophic entropy of indeterminate set, IM, is described as

$$En_{IM}(k) = -\sum_{k=\min\{IM\}}^{\max\{IM\}} p_{IM}(k) \ln p_{IM}(k) \tag{12}$$

where p_{IM} is the probability of indeterminate membership function. The goal of entropy is to eliminate uncertainty and fuzziness from images. It is employed to assess the intensities distribution for an image. If entropy is high, the gray levels have equal probability otherwise the gray levels have unequal probability resulted in a non uniform image. The values of IM is used to determine the indeterminate degree of element P_{NI}. The changes in TM in correlation with IM influence the distribution of element in IM and thus, vary the entropy of IM.

C. Proposed neutrosophic filtering operation

A filtering operation for pixel $\widehat{P(NI)}$ in neutrosophic domain is defined in Eq. (13).

$$\widehat{P(NI)} = P(TM, IM) \tag{13}$$

where $\widehat{P(NI)}$ is the pixel value, TM is true membership component in neutrosophic image and IM is the indeterminate membership subset in neutrosophic image. Further, pixels of $\widehat{\widehat{TM}}$ component are processed based on IM as represented in Eq. (14).

$$\widehat{\widehat{TM}} = \begin{cases} TM & IM < \chi \\ \widehat{TM} & IM \geq \chi \end{cases} \tag{14}$$

where χ is the indeterminacy threshold which is used to control the indeterminacy of image. If IM value is below χ then no filtering operation will be carried out on TM, or else, variational filtering on $\widehat{TM}$ given in Eq. (15) will be applied. The values of indeterminacy threshold parameter χ is determined by conducting various experiments on a set of images at different noise levels in neutrosophic domain. From experiments, it is observed that the maximum SNR value is obtained at $\chi = 1.2$ and it starts decreasing as values of χ goes beyond 1.2. Therefore, the value of χ is set to 1.2 by checking the optimal value at step interval of 0.1 from 0 to 10.

Then Neutrosophic domain Nakagami Total Variation filtering operation (NNTV) can be represented as

$$\widehat{TM} = \arg\min_{TM} \left\{ \sum_{\substack{1 \leq i \leq m, \\ 1 \leq j \leq n}} \underbrace{\left(2TM + \frac{1}{2\sigma^2} e^{2(f-TM)} \right)}_{\textit{fidelity term}} + \underbrace{\lambda \|\nabla TM\|_2}_{\textit{regularizer term}} \right\} \tag{15}$$

where f is the noisy image, $\|\nabla TM\|_2$ denotes an isotropic discrete total variation regularizer for the image and λ is the regularizer parameter used to balance the fidelity term and the regularization term. The fidelity term is derived from the assumption of Nakagami noise distribution. A regularizer term is used to smooth and preserve the edges efficiently in the homogeneous regions of an image. The above minimization problem (15) is solved by Chambolle's projection method and Augmented Lagrange method [7]. The value of λ is required to be experimentally set to an optimum value for different types

of applications. From experiments, it is observed that a higher value of λ yields a blurry, over-smoothed denoised image while suppressing speckle noise. Conversely, a smaller value of λ removes very modest amount of noise but enhances and preserves the details of small tissues. Therefore, value of λ is set to 0.83 for speckle reduction and edge preservation.

$$\widehat{IM} = \frac{\delta_{\widehat{TM}} - \delta_{\widehat{TM}_{\min}}}{\delta_{\widehat{TM}_{\max}}} \tag{16}$$

$$\delta_{\widehat{TM}} = abs(\widehat{TM} - \widehat{\widehat{TM}}) \tag{17}$$

where $\delta_{\widehat{TM}}$ is the absolute difference between $\widehat{TM}$ and $\widehat{\widehat{TM}}$ after χ operation. The details of solving Eq. (15) are given in [8].

D. Transformation of neutrosophic domain to gray level domain

After speckle reduction, finally neutrosophic image is transformed from neutrosophic domain to gray level domain by Eq. (18).

$$\hat{\hat{f}} = \hat{f}_{\min} + (\hat{f}_{\max} + \hat{f}_{\min}) \cdot \widehat{\widehat{TM}} \tag{18}$$

where $\hat{f}_{\min}$ is the minimum intensity value, $\hat{f}_{\max}$ is the maximum intensity value and $\widehat{\widehat{TM}}$ component is processed based on *IM* after applying neutrosophic variational filtering operation. The proposed Neutrosophic Nakagami Total Variation (NNTV) speckle reduction method can be implemented using Algorithm 1.

Algorithm 1 Proposed Neutrosophic domain speckle reduction method.

INPUT: Noisy image, f.

OUTPUT: Speckle suppressed image, $\hat{\hat{f}}$.

Set epsilon $(\varepsilon) = 1e{-}4$, iteration index $(k) = 0$.

Step 1: Transform image into neutrosophic domain using Eq. (7) to Eq. (11).

Step 2: Perform filtering operation given in Eq. (13) to Eq. (17) to obtain $\widehat{TM}$ and $\widehat{IM}$.

Step 3: Compute the entropy of the indeterminate subset $\widehat{IM}$ to obtain entropy $En_{IM}(k)$ by Eq. (12).

Step 4: If

$$\frac{En_{IM}(k+1) - En_{IM}(k)}{En_{IM}(k)} < \varepsilon,$$

Goto Step 5;

else

$TM = \widehat{TM}$ & $IM = \widehat{IM}$

Goto Step 2.

Step 5: Transform $\widehat{\widehat{TM}}$ of the neutrosophic domain into the gray level domain using Eq. (18).

4. Experimental results and discussion

This section demonstrates the results of experiments to evaluate effectiveness of proposed method in comparison to other speckle reduction methods. The methods are assessed on both synthetic and real ultrasound images. In experiments, performance of proposed neutrosophic domain speckle reduction (NNTV) method is compared with Nonconvex Sparse Regularizer Speckle Noise removal (NRSNR) [7], NTV [8] and Neutrosophic Nonconvex Sparse Regularizer Speckle Noise Removal (NNRSNR) [20] method.

Table 1
Comparison of different methods on img1 at different noise levels ($\sigma = 0.3$ to 0.9) in terms of SNR in dB.

Variance \ Methods	Noisy	NRSNR [7]	NNRSNR [23]	NTV [8]	NNTV
0.3	21.11	22.73	24.22	25.35	26.89
0.4	19.04	22.12	23.03	23.73	24.32
0.5	17.9	22.46	23.73	24.26	25.86
0.6	16.38	21.64	21.98	22.75	23.07
0.7	15.21	18.71	19.66	20.99	21.75
0.8	13.99	17.20	18.37	20.15	20.89
0.9	3.63	6.85	8.75	9.66	10.33
Average	**15.32**	**18.81**	**19.96**	**20.98**	**21.87**

4.1. Results and analysis on synthetic images

The quantitative evaluation of despeckling methods are conducted on synthetic images in which speckle noise is created using speckle simulation procedure. The effectiveness of the proposed NNTV method is assessed by carrying out various experiments on the speckled images at different noise variances from $\sigma = 0.3$ to 0.9. Table 1 represents the SNR values of noisy image, NTV, NRSNR, NNRSNR and NNTV for the phantom image (img1). From quantitative results, it is observed that the NNTV method outperformed the NRSNR, NNRSNR and NTV by gaining higher SNR value.

Similar type of observations has been made visually by the comparison of NRSNR, NTV, NNRSNR and proposed NNTV on speckle simulated phantom image (img1) as illustrated in Fig. 3. Fig. 3(a) illustrates a synthetic image and Fig. 3(b) displays the speckle simulated image. Whereas Fig. 3(c) illustrates that the NRSNR method blurred the necessary details such as edges of despeckled image. Fig. 3(d) reveals that the neutrosophic domain NNRSNR method carried out speckle suppression well. However, some of the pixels are advertently suppressed and blurred near the boundaries. Similar type of observation could be made by Fig. 3(e) and Fig. 3(f) that the NNTV method has better visual result as compared to other methods in terms of speckle removal and edge preservation.

Further to show edge and corner preservation, line profile is illustrated in Fig. 4. Fig. 4(a) shows speckle simulated image along with the highlighted line. Fig. 4(b) illustrates the line profile of original image in black colour in form of dotted line whereas line profile of speckle simulated image in form of dashed line in green colour. The line profiles of all despeckled images are shown in red colour to differentiate them with line profiles of original and noisy image. Fig. 4(c) shows the despeckled image filtered by NRSNR which demonstrate that speckle is not suppressed effectively, moreover, boundaries are also not preserved. However, NNRSNR has tried to preserve the edges with better speckle suppression but not able to preserve the textured area. It is also observed that NTV as shown in Fig. 4(e) has tried to preserve the edges with speckle reduction

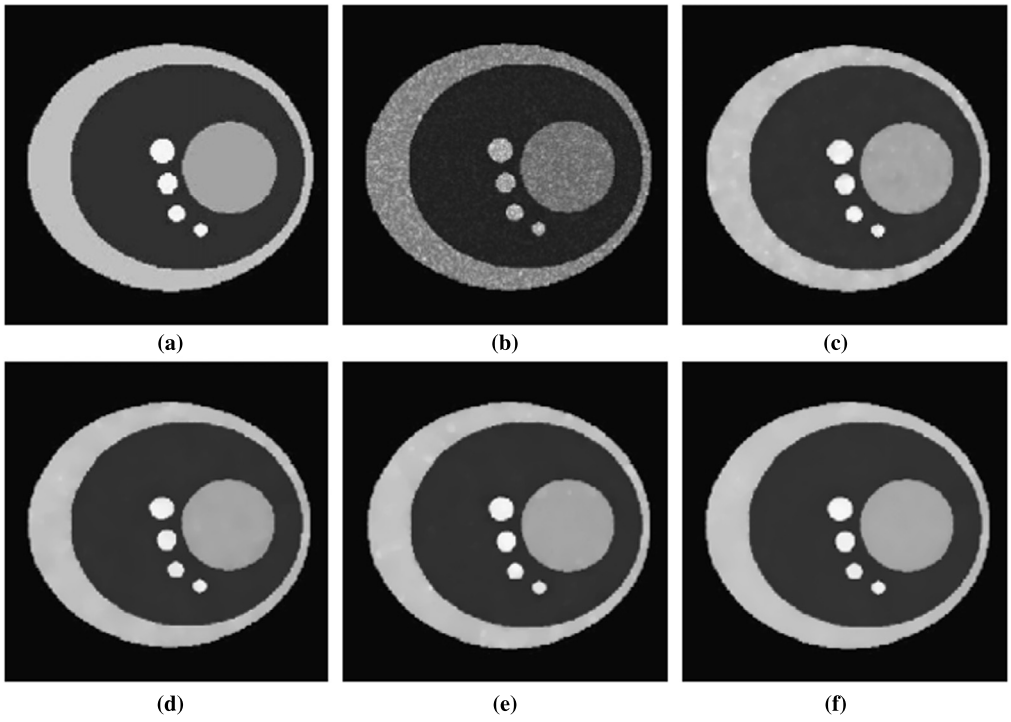

Fig. 3. **(a)** Original phantom image (img1), **(b)** speckle simulated image ($\sigma = 0.6$). Denoised results on image processed by **(c)** NRSNR [7], **(d)** NNRSNR [23], **(e)** NTV [8], **(f)** NNTV.

but not performed well in preserving the corners and texture due to noisy pixels. The indeterminate pixels cannot be handled by NTV and NRSNR effectively as noisy pixels and texture information are often intermixed due to indeterminacy. NNTV is able to handle the noisy pixels and texture information using true membership and indeterminate membership. The line profile of NNTV method as given in Fig. 4(f) shows that it can remove the speckle noise effectively with preserved edges and corners. It outperformed all other methods due to the integration of Nakagami variational model in neutrosophic domain. Hence, speckle suppression and edge preservation can be better achieved in neutrosophic domain using Nakagami statistics.

To supplement these results, VIF and UQI values of all methods on img2 (at ($\sigma = 0.6$)) are also plotted in Fig. 5(a). The EPI and MSSIM values on img2 are plotted in Fig. 5(b). The plots clearly revealed that the neutrosophic domain methods outperformed their counterparts in terms of VIF and UQI.

Table 2 with execution time. From tabular data, it is noticed that the NNTV method has achieved higher values of UQI, EPI, MSSIM and VIF followed by NNRSNR, NTV and NRSNR. Moreover, the NNTV method has taken a comparative less time (2.37 s) as compared to other methods and the efficiency of the neutrosophic domain methods are better as compared to spatial domain methods.

All these visual results with SNR values validate that the neutrosophic domain methods outperformed their counterparts in terms of quantitative measures and time complexity. The neutrosophic domain methods are also found effective in preservation of subtle details such as edges and texture of despeckled image similar to the original image with improved contrast. From results, it is concluded that the performance of speckle reduction methods in neutrosophic domain are better than the speckle reduction methods in spatial domain.

4.2. Results and analysis on real ultrasound images

This section presents the experimental results on original ultrasound images to evaluate NRSNR, NNRSNR, NTV and NNTV methods. As quantitative results cannot be taken on these images due to the non availability of noise free images, the visual analysis of real ultrasound images are shown with line profiles in this section. The real ultrasound image is shown in Fig. 6(a). Fig. 6(b) and Fig. 6(c) illustrate the visual results of NRSNR method and NTV method respectively. The visual results revealed that some of the important details have been lost and the contrast has been changed with speckle reduction.

The results of NNRSNR as shown in Fig. 6(d) shows that speckle noise is reduced efficiently but edges became slightly blurred. The NNRSNR method can preserve the nodule boundaries effectively while speckle removal but some minute details have been lost which are obscured under speckle. From results, it is observed that the NNTV method removed the speckle noise more effectively while preserving its original texture and highlighting the minute details as illustrated in Fig. 6(e). Also, NNTV improved the contrast between surrounding regions and nodule.

Fig. 7 shows the visual outcome of the NNRSNR and NNTV supplemented by their edge maps. The edge map is also utilized to detect and characterize the edges after speckle noise removal. From the analysis of denoised image, it is observed that the speckle reduction and edge preservation is better achieved by NNTV [Fig. 7(d)] in comparison to NNRSNR [Fig. 7(b)].

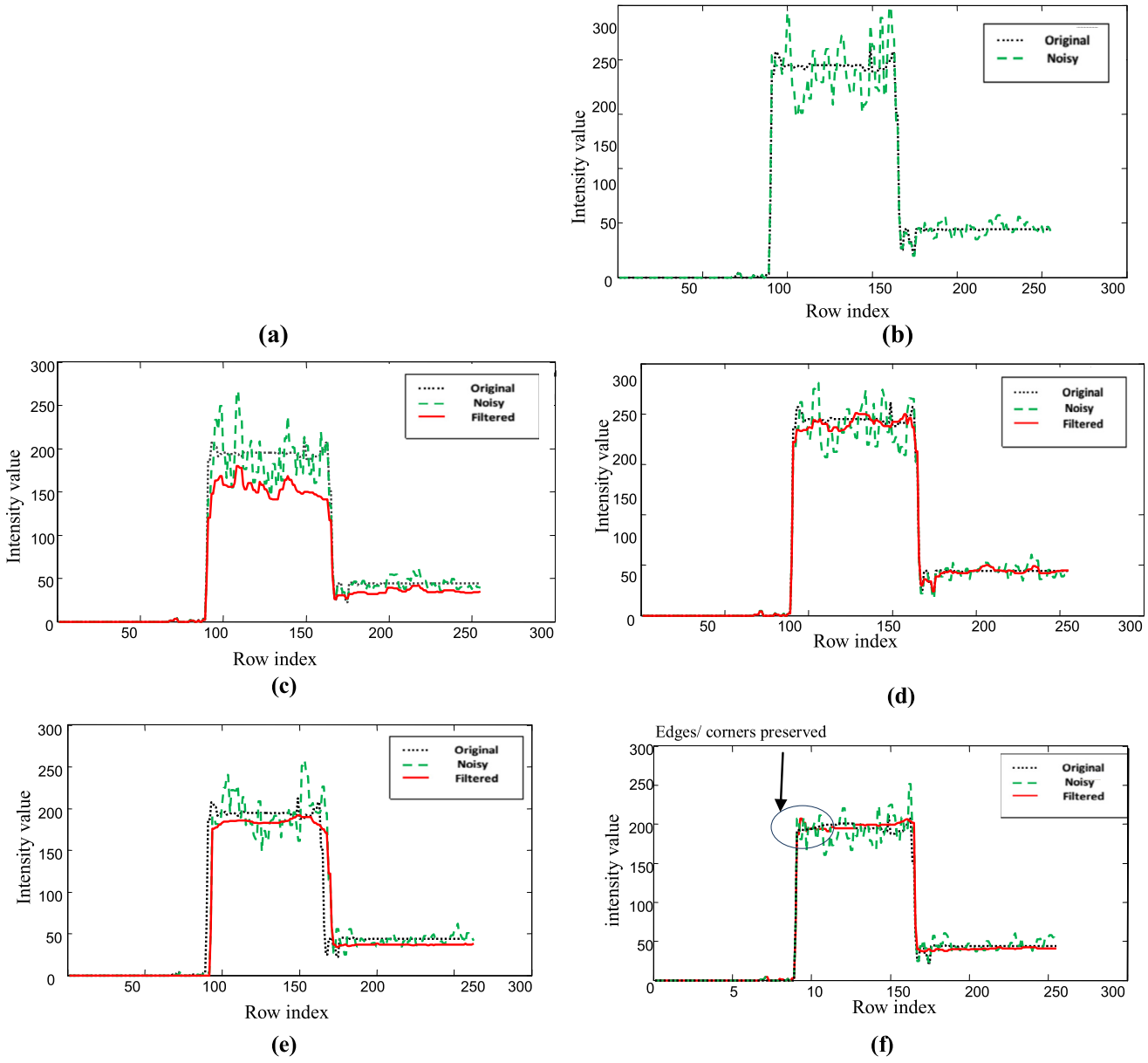

Fig. 4. Denoising results for the phantom image (img1) are shown via intensity profiles of images along highlighted line: **(a)** speckled image at variance 0.5, line profile of **(b)** original and noisy image, **(c)** NRSNR, **(d)** NNRSNR, **(e)** NTV, **(f)** NNTV. (For interpretation of the references to colour in this figure, the reader is referred to the web version of this article.)

The edge map of despeckled image obtained by NNTV method has shown that the boundary of nodule can be clearly distinguished from its adjoining parenchyma as illustrated in Fig. 7(e) as compared to edge map of NNRSNR as shown in Fig. 7(c). The visual outcomes of NRSNR, NTV, NNRSNR and NNTV are also evaluated as shown in Fig. 8.

Further, with a closer glance in Fig. 8(d) and Fig. 8(f), it has been observed that NNRSNR and NNTV methods surpass the other methods by clearly highlighting the edges of thyroid nodule with the suppression of speckle noise as well as with the preservation of edges and corners in the thyroid gland ultrasound image. The methods in neutrosophic domain are able to preserve the corners, boundaries and sharp features of original image. Also the minute subtle details which are hidden by speckle become noticeable in despeckled image processed by NNTV. It has been found that the NNTV method can better preserved the nodule's boundaries in thyroid ultrasound image while the degree of speckle suppression is high as compared to SNR method. It is also observed that the speckle is removed effectively and structure of thyroid nodule has been well preserved by NNTV method using Nakagami distribution statistics.

4.3. Evaluation by medical experts

Table 3 lists the Mean Opinion Score (MOS) for NRSNR, NNRSNR, NTV and NNTV obtained from medical experts. Total 13 images were randomly chosen from real ultrasound im-

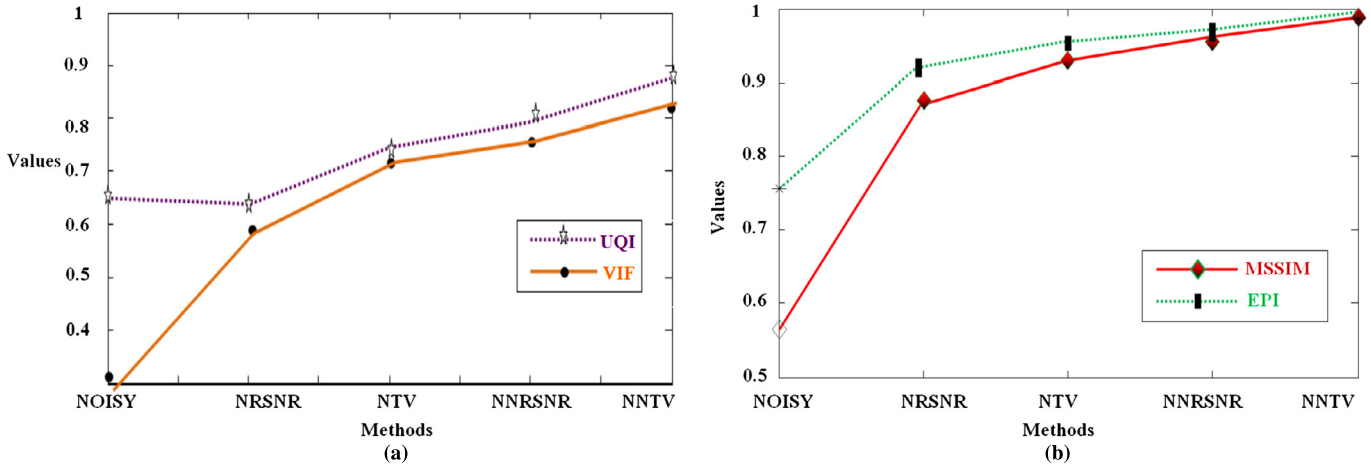

Fig. 5. Comparison of Noisy, NRSNR, NTV, NNRSNR and NNTV for image (img2) at ($\sigma = 0.6$) in terms of **(a)** VIF and UQI, **(b)** MSSIM and EPI.

Table 2
Comparison of different methods on img3 (at variance of 0.6) in terms of UQI, EPI, MSSIM, VIF and execution time.

Metrics / Methods	UQI	EPI	MSSIM	VIF	Time (s)
Noisy image	0.6653	0.6917	0.6581	0.2917	–
NRSNR	0.7026	0.8133	0.7678	0.3245	**2.30**
NNRSNR	**0.7902**	**0.8718**	**0.8099**	**0.3565**	**2.55**
NTV	0.7440	0.8505	0.7897	0.3667	2.12
NNTV	**0.8606**	**0.8813**	**0.8139**	**0.3771**	**2.37**

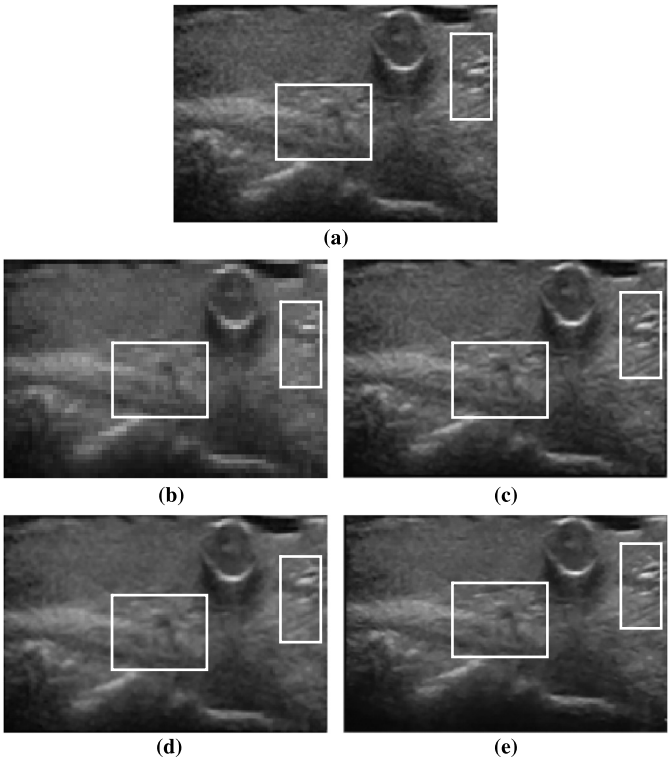

Fig. 6. **(a)** Original thyroid ultrasound image (img6). Image processed by **(b)** NRSNR, **(c)** NTV, **(d)** NNRSNR, **(e)** NNTV.

Table 3
Average mean opinion score assigned by each expert.

Methods / Experts	Original	NRSNR	NNRSNR	NTV	NNTV
Expert 1	1.46	4.23	4.53	4.76	4.84
Expert 2	1.84	3.07	3.53	3.69	3.92
Expert 3	1.53	3.92	3.76	4.15	4.46
Average MOS	**1.61**	**3.74**	**3.94**	**4.20**	**4.41**

ages. For each case, total 13 images were evaluated including one original and 10 filtered. The experts have assigned score in the 1–5 scale corresponding to low and high visual perception criteria. One is assigned to an image with the poor visual perception. The visual effectiveness of different methods was assessed on the basis of speckle suppression, boundaries or edges, resolvable details and nodule's anatomical structures preservation, improvement in visibility of small structures, and contrast enhancement between adjacent tissues and nodule. The experts identified the different anatomical structures and assigned the score to each processed image. The average value of score given for each method is calculated for each image by experts is reported in Table 3. The methods with lower value of MOS are not clinically acceptable and with higher values are clinically acceptable. For the experts as listed in Table 3, the best despeckled method is the NNTV with highest score followed by NTV, NNRSNR and NRSNR. The average score has shown that the highest value was assigned to the NNTV as it can make good balance between speckle removal and edge preservation due to the use of Nakagami statistics in neutrosophic domain.

5. Conclusions

In this work, variational method has been proposed in neutrosophic domain using Nakagami distribution for speckle reduction in ultrasound image. Initially, the image is transformed into neutrosophic domain by defining true, false and indeterminacy membership. The entropy in neutrosophic domain is used to assess the indeterminacy. A neutrosophic variational filtering operation based on Nakagami statistics is proposed to reduce the indeterminacy and speckle in the image. The pro-

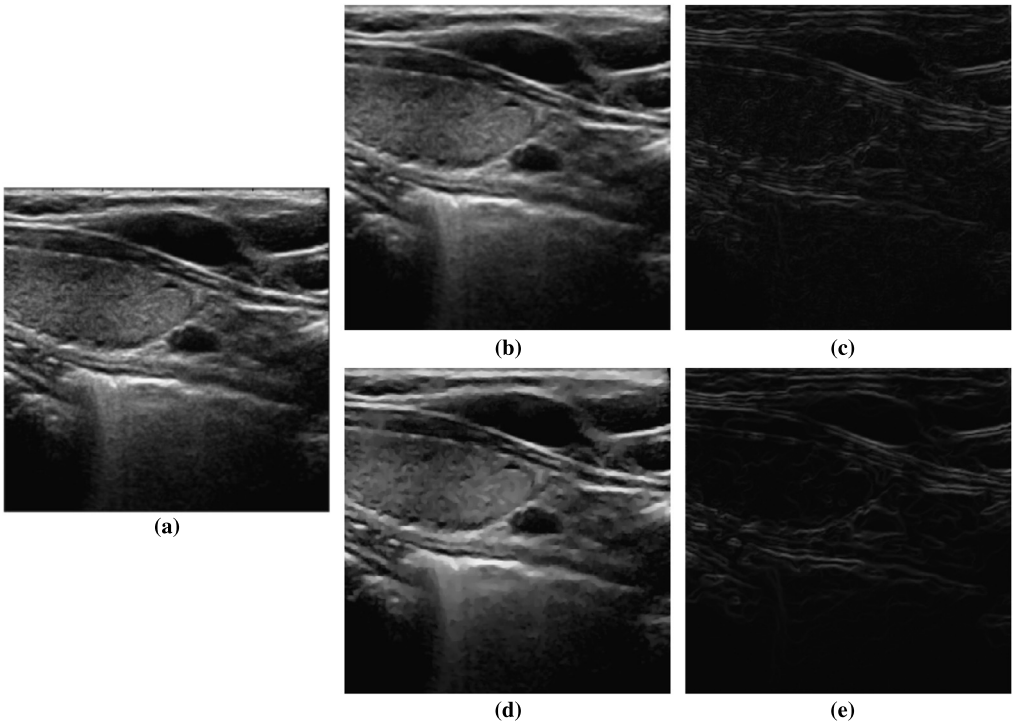

Fig. 7. Visual results on the thyroid ultrasound image (img4): **(a)** original image, **(b)** image processed by NNRSNR, **(c)** edge map of NNRSNR, **(d)** image processed by NNTV, **(e)** edge map of NNTV.

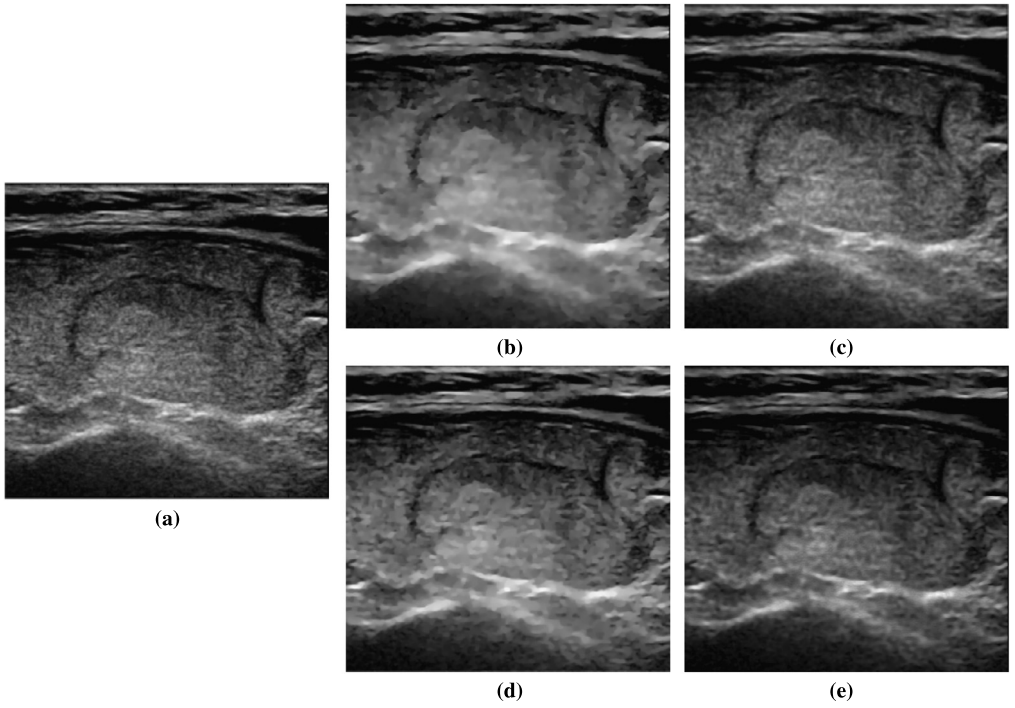

Fig. 8. Visual results on the thyroid ultrasound image (img9). **(a)** Original image. Denoised results on the image processed by **(b)** NRSNR, **(c)** NTV, **(d)** NNRSNR, **(e)** NNTV method.

posed method has been evaluated quantitatively using synthetic images by conducting various experiments at different noise levels and qualitatively using real ultrasound images. In experiments, the proposed method is evaluated with its counterpart to show the efficacy of neutrosophic domain. The proposed NNTV method performed better than NTV, NRSNR and NNRSNR in terms of SNR as listed in Table 1. Moreover, the values of edge preserving metrics such as VIF, EPI, UQI and MSSIM are also in favour of NNTV method [Table 2]. The NNTV method has an average SNR gain of 1.91 dB over NNRSNR. Medical ex-

perts also performed the subjective evaluation by computing the mean opinion score to show the robustness of proposed NNTV method. The proposed NNTV method has got score of 4.41 followed by NTV (4.2), NNRSNR (3.94) and NRSNR (3.74) out of 5 as given in Table 3. From results, it is observed that NNTV is able to handle the indeterminate pixels and preserve the valuable information such as texture and edges. Besides, neutrosophic domain methods are slightly more complex due to transformation of images in neutrosophic domain. Hence, NNTV method can assist endocrinologists in improving the quality of ultrasound images for accurate segmentation of thyroid nodules which is very important in Computer aided detection systems.

Conflict of interest statement

There is no conflict of interest.

References

[1] Kharchenko VP, Kotlyarov PM, Mogutov MS, Alexandrov YK, Sencha AN, Patrunov YN, et al. Ultrasound diagnostics of thyroid diseases. Springer Science & Business Media; 2010.

[2] Koundal D, Gupta S, Singh S. Survey of computer-aided diagnosis of thyroid nodules in medical ultrasound images, vol. 2. In: Proceedings of the second international conference on advances in computing and information technology, vol. 2. Springer AISC, vol. 177. 2012. p. 459–67.

[3] Rudin L, Lions PL, Osher S. Multiplicative denoising and deblurring: theory and algorithms. In: Osher S, Paragios N, editors. Geometric level sets in imaging, vision, and graphics; 2003. p. 103–19.

[4] Aubert G, Aujol JF. A variational approach to remove multiplicative noise. SIAM J Appl Math 2003;68:925–46.

[5] Shi J, Osher S. A nonlinear inverse scale space method for a convex multiplicative noise model. SIAM J Appl Math 2008;1(3):294–321.

[6] Han Y, Feng X, Baciu G. Nonconvex sparse regularizer based speckle noise removal. Pattern Recognit 2013;46:989–1001.

[7] Koundal D, Gupta S, Singh S. Nakagami-based total variation method for speckle reduction in thyroid ultrasound images. Proc Inst Mech Eng, H J Eng Med 2016;230(2):97–110.

[8] Keerthivasan A, Babu JJ, Sudha GF. Speckle noise reduction in ultrasound images using fuzzy logic based on histogram and directional differences. In: IEEE international conference on communication and signal processing; 2013. p. 499–503.

[9] Salama AA, Smarandache F, Elsa M. Introduction to image processing via neutrosophic techniques. Neutrosoph Sets Syst 2014;5:59–64.

[10] Guo Y, Cheng HD, Zhang Y, Zhao W. A new neutrosophic approach to image denoising. In: 11th joint conference on information science on computer vision, pattern recognition and image processing; 2008.

[11] Guo Y, Cheng HD, Zhang Y. A new neutrosophic approach to image denoising. New Math Nat Comput 2009;5(3):653–62.

[12] Mohan J, Krishnaveni V, Guo Y. A neutrosophic approach of MRI denoising. In: Proceeding of IEEE international conference on image information processing; 2011. p. 1–6.

[13] Mohan J, Krishnaveni V, Guo Y. Performance analysis of neutrosophic set approach of median filtering for MRI denoising. Int J Electron Commun Eng Technol 2012;3(2):148–63.

[14] Mohan J, Thilaga AP, Chandra S, Krishnaveni V, Guo Y. Image denoising based on neutrosophic Wiener filtering. In: Proceedings of the second international conference on advances in computing and information technology, vol. 2177. 2012. p. 459–67.

[15] Mohan J, Thilaga AP, Chandra S, Krishnaveni V, Guo Y. Evaluation of neutrosophic set filtering technique for image denoising. Int J Multimedia Appl 2012;4(4):73–81.

[16] Mohan J, Krishnaveni V, Guo Y. A new neutrosophic approach of Wiener filtering for MRI denoising. Meas Sci Rev 2013;13(4):177–86.

[17] Mohan J, Krishnaveni V, Guo Y. MRI denoising using nonlocal neutrosophic set approach of Wiener filtering. Biomed Signal Process Control 2013;8(6):779–91.

[18] Guo Y, Şengür A. A novel image segmentation algorithm based on neutrosophic filtering and level set. Neutrosoph Sets Syst 2013;46(1):122–6.

[19] Xianying Q, Liu B, Xu J. A neutrosophic filter for high-density salt and pepper noise based on pixel-wise adaptive smoothing parameter. J Vis Commun Image Represent 2016;36:1–10.

[20] Koundal D, Gupta S, Singh S. Speckle reduction method for thyroid ultrasound images in neutrosophic domain. IET Image Process 2016;10(2):167–75.

[21] Koundal D, Gupta S, Singh S. Speckle reduction filter in neutrosophic domain. In: Proceedings of international conference of biomedical engineering and assisted technologies; 2012. p. 786–90.

[22] Lee J. Digital image enhancement and noise filtering by use of local statistics. IEEE Trans Pattern Anal Mach Intell 1980;2(2):165–8.

[23] Kuan DT, Sawchuk AA, Strand TC, Chavel P. Adaptive restoration of images with speckle. IEEE Trans Acoust Speech Signal Process 1987;35(3):373–83.

[24] Pizurica A, Philips W, Lemahieu I, Acheroy M. A versatile wavelet domain noise filtration technique for medical imaging. IEEE Trans Med Imaging 2003;22(3):323–31.

[25] Sheikh HR, Bovik AC. Image information and visual quality image processing. IEEE Trans Image Process 2006;15(2):430–44.

[26] Wang Z, Bovik AC. A universal image quality index. IEEE Signal Process Lett 2002;9(3):81–4.

[27] Sattar F, Floreby L, Salomonsson G, Lovstrom B. Image enhancement based on a nonlinear multiscale method. IEEE Trans Image Process 1997;6(6):888–95.

[28] Wang Z, Simoncelli EP, Bovik AC. Multi-scale structural similarity for image quality assessment. In: IEEE Asilomar conference on signals, systems and computers, vol. 2; 2003. p. 1398–402.

[29] Smarandache F. A unifying field in logics: Neutrosophic logic. Neutrosophy, neutrosophic set, neutrosophic probability. third edition. American Research Press; 2003.

[30] Shan J, Cheng HD, Wang Y. A novel segmentation method for breast ultrasound images based on neutrosophic l-means clustering. Med Phys 2012;39(9):5669–82.

[31] Koundal D, Gupta S, Singh S. Computer aided thyroid nodule detection system using medical ultrasound images. Biomed Signal Process Control 2018;40:117–30.